Real-Time Video Transmission over Different Underwater Wireless Optical Channels Using Directly Modulated 520 nm Laser Diode

Abdullah Al-Halafi, *Student Member, IEEE*, Hassan Makine Oubei, *Member, IEEE*, Boon S. Ooi, *Senior Member, IEEE*, and Basem Shihada, *Senior Member, IEEE*

***Abstract*—We experimentally demonstrate a high quality real-time video streaming over an underwater wireless optical communication (UWOC) link up to 5 m distance using PSK and QAM modulation schemes. The communication system uses software defined platforms connected to a commercial TO-9 packaged pigtailed 520 nm directly modulated laser diode (LD) with 1.2 GHz bandwidth as the optical transmitter and an avalanche photodiode (APD) module as the receiver. To simulate various underwater channels, we perform laboratory experiments on clear, coastal, harbor I, and harbor II ocean water types. The measured bit error rate of the received video streams is 1.0*10^{-9} for QPSK, 4-QAM and 8-QAM, and 9.9*10^{-9} values for 8-PSK. We further evaluate the quality of the received live video images using Structural Similarity (SSIM) and achieve values of about 0.9 for the first three water types, and about 0.7 for harbor II. To the best of our knowledge, these results present the highest quality video streaming ever achieved in UWOC systems that resemble communication channels in real ocean water environments.**

***Index Terms*—Underwater communication, optical communication, video, diode lasers, PSK, QAM.**

I. Introduction

TWO thirds of our planet is covered with oceans that have vast resources critical to our living. Exploring and monitoring such resources with real-time video has huge potentials in serving many underwater applications. As when the situation entails critical, tactic and time sensitive operations, underwater systems need to be equipped with ultrafast wireless communication solutions for the realization of live video streaming as an ultimate tool to virtually mimic the reality of that unseen environment. Another example is the inspection and maintenance of huge network of subsea pipelines, cables and steel structures for the offshore oil and gas fields. Wireless solutions become essential alternatives for inspecting parts of those fields in shallow water, where large barges cannot approach near surface locations to carry a remotely operated vehicle (ROV). Current methods are difficult and costly as divers are constrained by the work hours and depths, and the accompanying boats remain costly to operate and subject to permissions of weather [1].

Existing technologies such as acoustic communication are widely deployed underwater but are generally limited by their low data rates (in Kbps) not sufficient for real-time and good quality video streaming [2]. The RF waves are also not suitable as they become strongly attenuated underwater [3]. Low frequencies (300 Hz) may propagate underwater but require large antenna and consume high transmission power [4]. As a promising alternative, underwater wireless optical communication (UWOC) offers much higher bandwidth enough to stream live video. In addition, due to the ease of deployment, low power consumption, much faster data rates, and increased security UWOC is becoming a preferred option. Nevertheless, it has also its own challenges and is still in its infancy. Underwater absorption, scattering, and turbulence are the key factors that significantly affect the performance of UWOC links and image-quality of underwater video and imaging systems [5]–[7]. As a matter of fact, only short range links have been established for UWOC [8]–[12].

The research on underwater video transmission has been sparse and only few studies have been reported. In 2005, Chancey established a 10 Mbps UWOC based video link over 4.6 m clear water channel [13]. In 2007, Baiden et al. [14] also constructed a 10 Mbps untethered telerobotic system to transmit video information underwater over a 10 m range on Long Lake in Sudbury, Ontario. The AquaOptical II video transmission system device [15] was based on an array of 18 light-emitting diodes (LEDs) transmitter and has a bandwidth limit of 4 Mbps. Moreover, a UWOC video system with externally modulated data in a varying water tank visibility was demonstrated in [16]. Those aforementioned research projects have established and shown the feasibility of underwater video streaming. However, those studies did not provide a systematic analysis to investigate the ef-

fects of various underwater channel conditions, resulting from changing the water turbidity levels, on video quality and when different modulation techniques are used.

In this paper, we evaluate the performance of a low-power, cost-effective, and UWOC based real-time video system employing Quadrature Amplitude Modulation (QAM) and Phase-Shift Keying (PSK) modulations. We take into account various underwater channel link conditions and analyze both overall Bit Error Rate (BER) and video quality. Performance results reveal that live video streaming is not only feasible over different ocean water types but also with good image quality.

The rest of this paper is organized as follows. In Section II, the system model is presented. In Section III, the experimental setup for both video transmission system and underwater wireless optical system are described. The experimental results and discussions are presented in Section IV. Finally, the paper is concluded in Section V.

II. System model

The video streaming system is built on universal software radio peripheral-reconfigurable input/output (USRP-RIO). LabVIEW software interface allows users to reconfigure and operate this hardware to suit our desired video application. When live video streams are captured via a DirectShow compliant webcam, the acquisition attributes are configured through NI-MAX software for the recommended resolution of 320 x 240 pixels. NI Vision Acquisition performs the various media processes, from detecting the camera, opening the camera session, to fetching the video streams from the camera into the host PC. The video streaming bits are assembled in 128 bit-message length, and built into packets with 30 guard bits, followed by 30 synchronization bits, the 128 message bits, and ending with 70 pad bits. Fig. 1 shows the video packet size and structure.

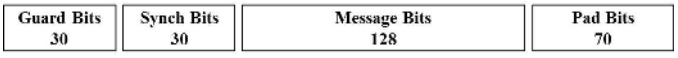

Fig. 1: Video packet length.

The packets are then modulated and transmitted by one USRP device into the laser diode through the underwater channel. When the packets are received by the photodetector then arrive into the second USRP receiver, they go under resampling and matched filter, demodulation, and detection of synchronization bits. The video packets are then displayed on the host PC. This digital communications model is shown in Fig. 2.

The overall system performance is evaluated using the measured BER. It is the ratio of the number of erroneous

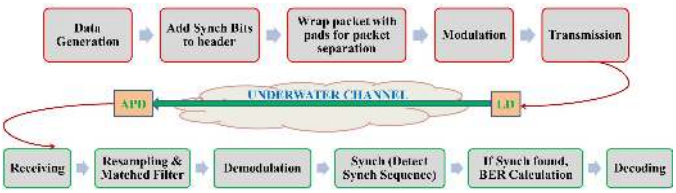

Fig. 2: Digital communications model for the transmitter and the receiver.

bits to the number of true bits following a trigger in the current input bit stream which is the Synch bits in our case. This measurement is based on 100K samples from the output of the *MT Calculate BER after Trigger (PN Sequence)* library [17].

III. Experimental setup

The actual photograph of the underwater real-time video transmission system setup is shown in Fig. 3. We utilize a 15 mW commercially available, TO-9 packaged and single-mode fiber-pigtailed green LD (Thorlabs LP520-SF15) as the optical transmitter.

Fig. 4 presents the light-current-voltage (L-I-V) curves of the pigtailed green LD having a threshold current of 58 mA, and a slope efficiency of around 16.7%. Fig. 5 shows the emission spectra of the LD under different injection currents obtained using a high-resolution spectrometer (Ocean Optics HR4000). The full-width at half-maximum (FWHM) of the LD is 0.45 nm. The emission center wavelength at 70 mA is around 515.2 nm and slightly changes with increasing injection current.

The video packets from the first USRP transmitter were superimposed on the DC laser bias current using the built-in Bias-Tee RF input within the laser driver mount (Thorlabs LDM9LP). The output radiation of the LD was collimated by a plano-convex lens (Thorlabs LA1951-A) of 25.4 mm diameter and 25.4 mm focal length to produce a parallel beam which is incident on the underwater channel. The underwater channel was simulated using a water tank made of polyvinyl chloride (PVC) with 1 x 0.6 x 0.6 m^3 dimensions. The tank was filled with municipality fresh tap water with an estimated attenuation coefficient = 0.071 m^{-1} [18], which is similar to the clear blue ocean water type. The optical path length in the water tank was extended up to 5 m using mirrors installed at both ends of the tank. After propagating through the water tank, the optical beam was focused into a high sensitivity silicon avalanche photodiode (Menlo Systems APD210) receiver unit using a 75 mm focal length lens (Thorlabs LA1608-A). The APD has 1 GHz cut-off bandwidth, 0.5 mm active diameter, 0.4 pW/$Hz^{1/2}$ noise equivalent power (NEP),

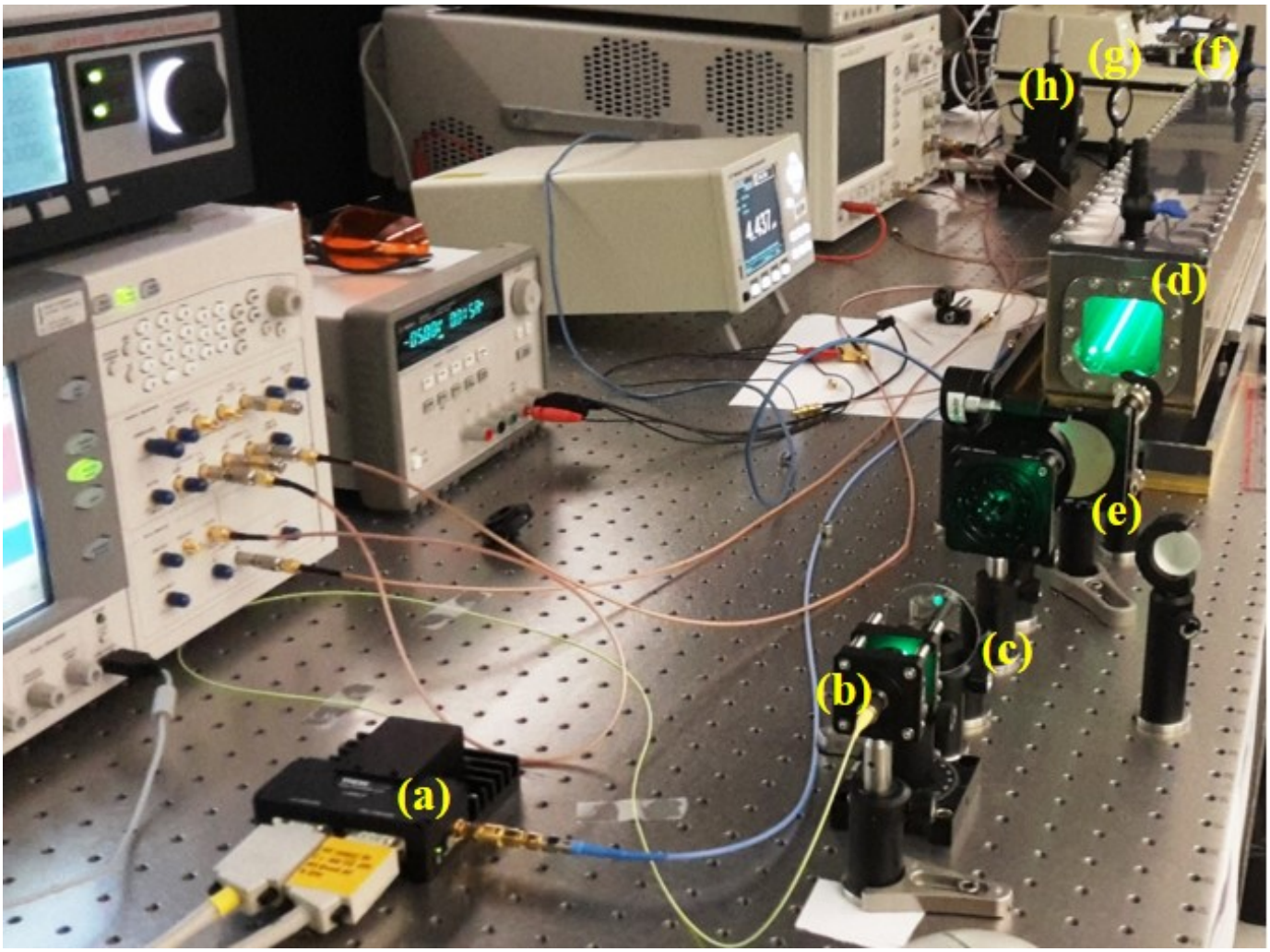

Fig. 3: Actual photograph of the water tank showing: (a) laser driver mount, (b) collimator lens, (c) attenuator, (d) green laser beams, (e) mirrors, (f) mirrors , (g) focusing lens, (h) avalanche photodiode (APD).

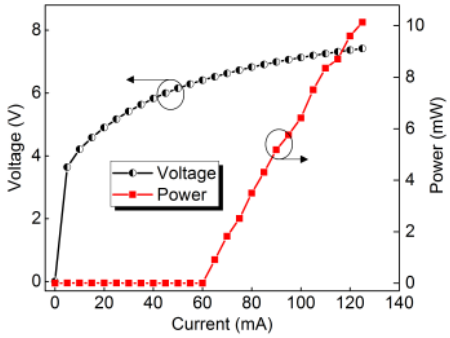

Fig. 4: Characteristics of the 520 nm LD at 25°C: L-I-V curves.

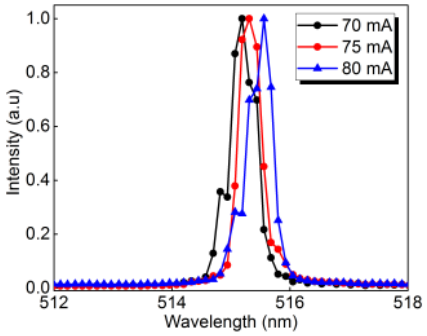

Fig. 5: Characteristics of the 520 nm LD at 25°C: optical spectra with increasing bias currents.

and around 13 A/W responsivity at 520 nm. The video signal is finally received by the second USRP receiver for interface and processing by the host PC through a PCI-E x 4Gbit/s cables.

Fig. 6 depicts the schematics of the overall system. All measurements were taken under normal room illumina-

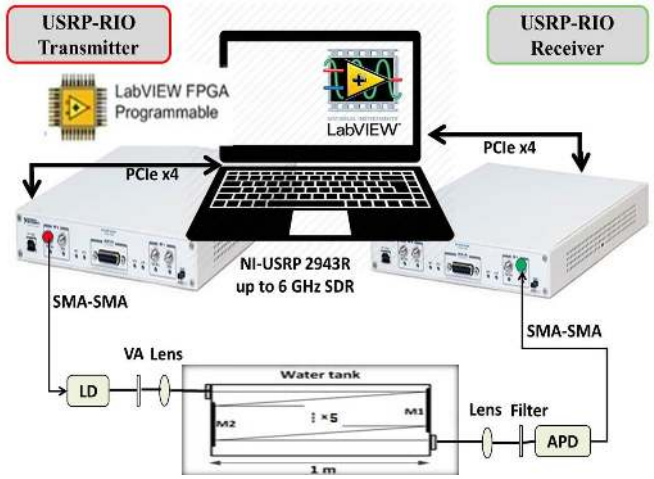

Fig. 6: Schematics of the underwater video streaming system over a reconfigurable wireless optical link, SMA: SubMiniature version A connectors, SDR: Software Defined Radio.

tion conditions. The water turbidity level is changed by adding accurate Maalox® solution based on [19] in an orderly fashion, in order to simulate various underwater channels as in Table I. The amounts of Maalox® concentration added to achieve the desired absorption and scattering coefficients corresponding to the clear, coastal, harbor I and harbor II water types, respectively, are shown in the last column of Table I. After the addition of each Maalox® concentration, we sufficiently stirred the mixture to obtain a uniform water channel before proceeding with the measurements.

TABLE I:
Representative absorption, scattering and total attenuation coefficient values based on [20]

Water Type	a (m^{-1})	b (m^{-1})	c (m^{-1})	V(μL)
Clear water	0.114	0.037	0.151	29.2
Coastal water	0.179	0.219	0.398	75.6
Harbor I water	0.187	0.913	1.10	198.1
Harbor II water	0.366	1.824	2.19	383.6

IV. Experimental Results and Discussions

Fig. 7 shows the eye diagrams, constellation maps, and received video images for clear water channel conditions under 8-PSK modulation and Fig. 8 for 8-QAM modulation. For simplicity, we show representative samples of the results. We observe that the eye diagrams are open for both modulations. The constellation maps are fairly distinguishable and we observe clear images.

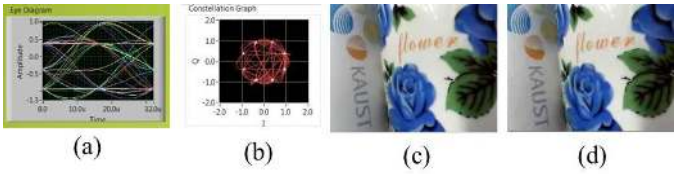

Fig. 7: Clear water: (8-PSK) (a) eye diagram, (b) constellation graph, (c) transmitted video, (d) received video.

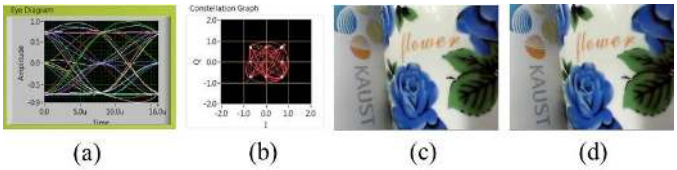

Fig. 8: Clear water: (8-QAM) (a) eye diagram, (b) constellation graph, (c) transmitted video, (d) received video.

We further investigated video transmission in coastal and harbor I waters. We found that the eye diagrams and constellation maps for each modulation were similar to clear water channel conditions. In Fig. 9, we present transmitted and received video images for 8-PSK and 8-QAM modulations for coastal water. We also show the results for harbor I in Fig. 10 for both 8-PSK and 8-QAM modulations. High quality and colored videos were obtained for both coastal and harbor I waters. However, there is a little distortion that is hardly noticed only when using 8-PSK at the right bottom corner of Fig. 9(b). It is corrected immediately and seamlessly on the next packet retransmission. This is an indication that 8-PSK suffers the most and this fact prevails in the next findings while we increase water turbidity as in harbor II.

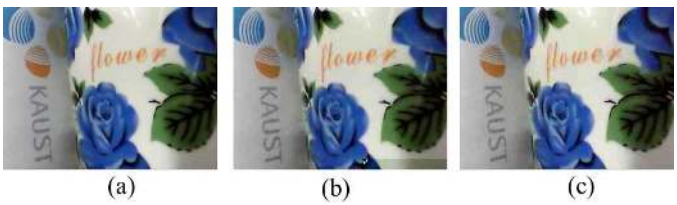

Fig. 9: Coastal water: (a) transmitted video; received videos for: (b) 8-PSK, (c) 8-QAM.

Finally, we studied video transmission quality in highly turbid harbor II water. Fig. 11 illustrates the received images next to the transmitted image for all modulations. As seen in Fig. 11(b), 8-PSK on harbor

Fig. 10: Harbor I water: (a) transmitted video; received videos for: (b) 8-PSK, (c) 8-QAM.

II ocean water type suffers the most. Fig. 11(c) shows that the received video also suffers from minor distortion at the bottom with 8-QAM, but is still better than 8-PSK. Although these are intermittent results and videos become clear again using retransmissions, but for the sake of completeness, we thought it provides an idea about the performance of the system at the most turbid water (i.e. harbor II).

Fig. 11: Harbor II water: (a) transmitted video; received videos for: (b) 8-PSK, (c) 8-QAM.

When we go from clear water to harbor II, the turbidity increases and the optical signal gets significantly absorbed and scattered. In the case of 8-QAM modulation scheme the constellation regions on the complex plane are larger and the boundaries are looser. Hence, it outperforms 8-PSK as the probability that one constellation point falls into the adjacent region or incorrect boundary is higher for 8-PSK; especially when the channel attenuation is very high as in the case of harbor II. Another advantage of using higher orders of QAM is that it is able to carry more bits of information per symbol but is less resilient to higher noise. As shown in Fig. 11, the video color, quality and the resolution are not significantly affected by the increased turbidity of the water. Note however that the water channel may have visual influences on the colored video when the link distances increase to longer ranges [21].

To evaluate the overall performance of the video transmission system, we present the average BER in Fig. 12. The BER increases with turbidity of the water, however the increase is evident when transmitting video in the most turbid harbor II water. Here we can see that all modulations achieved 1.0*10^{-9} BER except for 8-PSK which resulted in [1.43, 3.9, 4.3, and 9.9]*10^{-9} in clear, coastal, harbor I, and harbor II, respectively.

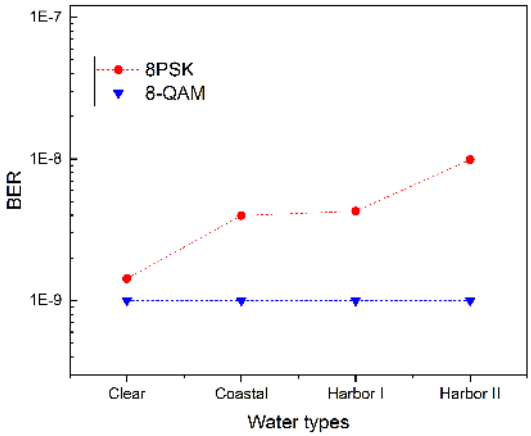

Fig. 12: BER of received videos.

In order to quantitatively assess the effects of using different water types and modulations on the received video quality, we use Structural Similarity (SSIM) method for quality analysis of the received video images based on the work of [22]. This quality metric assesses the visual impacts of luminance, contrast and structure of an image. Eq. (1) shows a multiplicative combination of the three aspects.

$$SSIM(xy) = [l(x,y)]^{\alpha} + [c(x,y)]^{\beta} + [s(x,y)]^{\gamma} \quad (1)$$

The luminance effects are calculated using local means, standard deviations, and cross-covariance for video images x and y as in Eq. (2)

$$L_{xy} = \frac{(2\mu_x\mu_y + C_1)}{(\mu_x\mu_x + \mu_y\mu_y + C_1)} \quad (2)$$

where $C_1 = (K_1 * 255)^2$. Similarly, the contrast effects are calculated as in Eq. (3)

$$C_{xy} = \frac{(2s_xs_y + C_2)}{(s_xs_x + s_ys_y + C_2)} \quad (3)$$

where $C_2 = (K_2 * 255)^2$. Finally, the structure comparison becomes as in Eq. (4)

$$S_{xy} = \frac{(r_{xy} + C_3)}{(s_xs_y + C_3)} \quad (4)$$

where $C_3 = C_2/2$. Here K_1 and K_2 are chosen to be K_1=0.3 and K_2=0.9. When the exponents are set to the default value $\alpha = \beta = \gamma = 1$, and $C_3 = C_2/2$, then the SSIM index formula simplifies to Eq. (5).

$$SSIM(xy) = \frac{(2\mu_x\mu_y + C_1).(2\sigma_{xy} + C_2)}{(\mu_x^2 + \mu_y^2 + C_1).(\sigma_x^2 + \sigma_y^2 + C_2)} \quad (5)$$

Based on this, offline algorithms were used to compare the similarity of the transmitted and its corresponding received video. In Fig. 13, SSIM is about 88%-96% for all modulations over the clear, coastal and harbor I. At harbor II, the corresponding SSIM of all modulations drop down except for 8-QAM which remains at around 95%. As stated earlier, as more bits per symbol are represented in higher order modulations, we increase the spectral efficiency. However, in this noisy channel, the probability of error increases for the correct placement of points on the constellation graph in 8-PSK, and although its corresponding SSIM is about 70%, it still has the lowest similarity index resulting in the most distorted video image of all used modulation schemes.

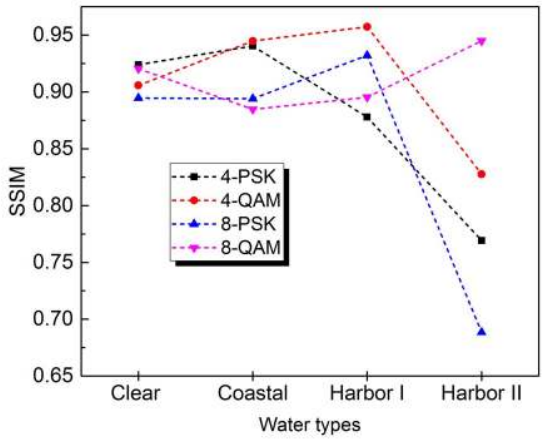

Fig. 13: SSIM results for video images.

V. Conclusion

In this work, we experimentally demonstrated a reconfigurable and cost-effective communications system for underwater live video streaming using wireless optical communications link. We evaluated our system using a testbed experiment over 5 m distance using four modulation techniques in four ocean water types. The video streaming system utilizes USRP-RIO hardware and LabVIEW software packages. This is integrated into the wireless optical transmission link which uses a commercially available TO-9 packaged pigtailed 520 nm LD as the transmitter and an APD module as the receiver. The live video transmission has been demonstrated and proven to be reliable resulting in open eye diagrams, clear constellation points and BER of $1.0*10^{-9}$ for clear, coastal, harbor I, and harbor II for all modulations, and $9.9*10^{-9}$ for 8-PSK. The quality of the received video was additionally evaluated using SSIM metric which resulted in values up to 96% similarity for all water types and about 70% for harbor II, indicating a very high similarity between the sent and received videos. Our comprehensive study on real-time video transmission over different ocean water types and various modulation techniques paves the way for designing better UWOC systems for next-generation underwater video applications.

References

[1] H. Kaushal and G. Kaddoum, "Underwater optical wireless communication," *IEEE Access*, vol. 4, no. 4, pp. 1518–1547, 2016.

[2] J. Ribas, D. Sura, and M. Stojanovic, "Underwater wireless video transmission for supervisory control and inspection using acoustic OFDM," in *Proc. of Oceans 2011 IEEE-Spain*. IEEE, 2011, pp. 1–9.

[3] Z. Zeng, H. Zhang, Y. Dong, and J. Cheng, "A survey of underwater optical wireless communications," *IEEE Commun. Surveys and Tutorials*, vol. 19, no. 1, pp. 204–238, 2017.

[4] U. S. N. fact file. (2001. [Accessed: May- 2017]) Extremely Low Frequency Transmitter Site Clam Lake, Wisconsin. [Online]. Available: https://fas.org/nuke/guide/usa/c3i/fs_clam_lake_elf2003.pdf

[5] W. Hou, "A simple underwater imaging model," *Opt. Letters*, vol. 34, no. 17, pp. 2688–2690, 2009.

[6] M. V. Jamali, P. Khorramshahi, A. Tashakori, A. Chizari, S. Shahsavari, S. AbdollahRamezani, M. Fazelian, S. Bahrani, and J. A. Salehi, "Statistical distribution of intensity fluctuations for underwater wireless optical channels in the presence of air bubbles," in *2016 Iran Workshop on Communication and Information Theory (IWCIT)*, May 2016, pp. 1–6.

[7] H. M. Oubei, E. Zedini, R. T. ElAfandy, A. Kammoun, M. Abdallah, T. K. Ng, M. Hamdi, M.-S. Alouini, and B. S. Ooi, "Simple statistical channel model for weak temperature-induced turbulence in underwater wireless optical communication systems," *Opt. Lett.*, vol. 42, no. 13, pp. 2455–2458, Jul 2017. [Online]. Available: http://ol.osa.org/abstract.cfm?URI=ol-42-13-2455

[8] K. Nakamura, I. Mizukoshi, and M. Hanawa, "Optical wireless transmission of 405 nm, 1.45 Gbit/s optical IM/DD-OFDM signals through a 4.8 m underwater channel," *Opt. Exp.*, vol. 23, no. 2, pp. 1558–1566, 2015.

[9] H. Oubei and et al., "4.8 Gbit/s 16-QAM-OFDM transmission based on compact 450-nm laser for underwater wireless optical communication," *Opt. Exp.*, vol. 23, no. 18, pp. 23 302–23 309, 2015.

[10] C. Shen and et al., "20-meter underwater wireless optical communication link with 1.5 Gbps data rate," *Opt. Exp.*, vol. 24, no. 22, pp. 25 502–25 509, 2016.

[11] H.-H. Lu and et al., "An 8 m/9.6 Gbps underwater wireless optical communication system," *IEEE Photonics J.*, vol. 8, no. 5, pp. 1–7, 2016.

[12] W. Tsai-Chen and et al., "Blue laser diode enables underwater communication at 12.4 Gbps," *Scientific Reports*, no. 7:40480, 2017.

[13] M. A. Chancey, "Short range underwater communication links," *Master thesis, North Carolina State Uni. (2005)*, 2005.

[14] G. Baiden and Y. Bissiri, "High bandwidth optical networking for underwater untethered telerobotic operation," in *Proc. of IEEE Oceans 2007*. IEEE, 2007, pp. 1–9.

[15] M. Doniec, A. Xu, and D. Rus, "Robust real-time underwater digital video streaming using optical communication," in *Proc. of IEEE Intl. Conf. on Robotics and Automation*. IEEE, 2013, pp. 5117–5124.
[16] M. Sun, B. Zheng, L. Zhao, X. Zhao, and F. Kong, "A design of the video transmission based on the underwater laser communication," in *Proc. of IEEE 2014 Oceans St. Johns*. IEEE, 2014, pp. 1–4.
[17] NI Product Manual, *MT calculate BER after trigger (PN Sequence)*, 2017. [Accessed: May- 2017]. [Online]. Available: http://www.ni.com/documentation/en/labview-comms/1.0/mt-node-ref/mt-calculate-ber-after-trigger-pn/
[18] J. W. Giles and I. N. Bankman, "Underwater optical communications systems. Part 2: basic design considerations," in *Proc. of IEEE Military Comm. Conf.*, vol. 3. IEEE, 2005, pp. 1700–1705.
[19] A. Laux and et al., "The abc's of oceanographic lidar predictions: a significant step toward closing the loop between theory and experiment," *J. Modern Opt.*, vol. 49, no. 3–4, pp. 439–451, 2002.
[20] T. J. Petzold, "Volume scattering functions for selected ocean waters," *Tech. Rep., SIO Ref. 72-78, Scripps Institution of Oceanography Visibility Laboratory, San Diego, Calif.*, pp. 1–79, 1972.
[21] S. Tang, Y. Dong, and X. Zhang, "Impulse response modeling for underwater wireless optical communication links," *IEEE Trans. Comm.*, vol. 62, no. 1, pp. 226–234, 2014.
[22] Z. Wang, A. Bovik, H. Sheikh, and E. Simoncelli, "Image quality assessment: from error visibility to structural similarity," *IEEE Trans. on Image Processing*, vol. 13, no. 4, pp. 600–612, 2004.

Abdullah Al-Halafi received his B.Sc. in Electrical Engineering from King Fahd University of Petroleum and Minerals (KFUPM), Saudi Arabia in (2003) and M.Sc. in Electronics and Electrical Engineering from the University of Glasgow, (Scotland, UK) in (2006). Currently, he is pursuing his Ph.D. at King Abdullah University of Science and Technology (KAUST), Saudi Arabia. Prior to KAUST, he worked on engineering and projects management of various large scale communications and control systems projects at SABIC, ABB and Saudi Aramco, Saudi Arabia. His research interests include underwater wireless optical networks, wireless sensor networks and queuing systems.

Hassan Makine Oubei is a PhD Student at the Computer, Electrical and Mathematical Sciences and Engineering at (KAUST). He received the B.S (2007) degree in Electrical Engineering from the City College of New York, USA. He joined Corning Incorporateds research and development division in Corning, New York where he worked as Opto-Electronics Engineer to develop synthetics green lasers for display applications (2007-2011) and Process Measurements Engineer (2011-2013). While working for Corning, Hassan also obtained his M.S (2010) degree in Electrical Engineering from Binghamton University in Binghamton, New York. His research interests include underwater wireless optical communications, optical fiber communications, underwater optical channel modeling, electro-absorption modulators based on InGaN/GaN quantum structures.

Boon S.Ooi is a Professor of Electrical Engineering at KAUST. He is also the Director of KACST - Technology Innovation Center (TIC) for Solid-State Lighting. Professor Ooi received the B.Eng. and Ph.D. degrees in electronics and electrical engineering from the University of Glasgow (Scotland, U.K) in 1992 and 1994, respectively. He joined KAUST from Lehigh University (Pennsylvania, USA) where he held an Associate Professor position and headed the Photonics and Semiconductor Nanostructure Laboratory. His research is primarily concerned with the study of semiconductor lasers and photonic integrated circuits. Specifically, he has contributed significantly to the development of practical technologies for semiconductor photonics integrated circuits and the development of novel broadband semiconductor lasers, multiple-wavelength lasers, and superluminescent diodes. Most recently, he focuses his research on the areas of GaN-based nanostructures and lasers for applications such as solid-state lighting and visible light communications. He has given many lectures, seminars and invited talks at universities, research institutions, and international conferences. He has been the organizing chair for several IEEE, OSA and MRS conferences, and served on the technical program committee of CLEO, IPC, and IEDM. He was an associate editor of IEEE Photonics Journal from 2009-2015 and has been as associate editor of SPIE Journal of Nanophotonics since 2015, and an associate editor for Optics Express since 2017. In KSA, he has founded the IEEE Photonics Society Western Saudi Arabia Chapter and been serving as the Chapter Chair since 2010. He has also been serving in the executive board member of IEEE Western Saudi Arabia Section since 2010. He was invited to present in COP18/CMP8 (The 18th Conference of Parties, and the 8th session the Meeting of the Parties to the Kyoto Protocol), United Nation Global Climate Change Conference (UN-GCC) in Doha in November 2012, and COP22 (The 18th Conference of Parties) in Marrakech in December 2016. Dr. Ooi is a Fellow of the International Society for Optics and Photonics (SPIE) and a Fellow of the Institute of Physics (UK), and a Senior Member of IEEE.

Basem Shihada is an Associate Professor of Computer Science and by courtesy Electrical Engineering at KAUST. He received his PhD from University of Waterloo in 2007. He joined Stanford University as a visiting faculty in Stanford Computer Science in 2008. He has been actively working on networking systems. Particularly interested in identifying the performance patterns for existing wireless network infrastructures and rebuild them to enhance their energy consumption, resource allocation, and reduce the associated performance delays. His current research covers a wide range of topics in broadband wired and wireless communication networks, including multi-hop, sensor, and cognitive networks. He is also interested in fiber-wireless network integration, optical networks, and green communication protocols.